Article

O and Si NMR Parameters of MgSiO Phases from High-Resolution Solid-State NMR Spectroscopy and First-Principles Calculations

Sharon E. Ashbrook, Andrew J. Berry, Daniel J. Frost, Alan Gregorovic, Chris J. Pickard, Jennifer E. Readman, and Stephen Wimperis

J. Am. Chem. Soc., **2007**, 129 (43), 13213-13224• DOI: 10.1021/ja074428a • Publication Date (Web): 09 October 2007

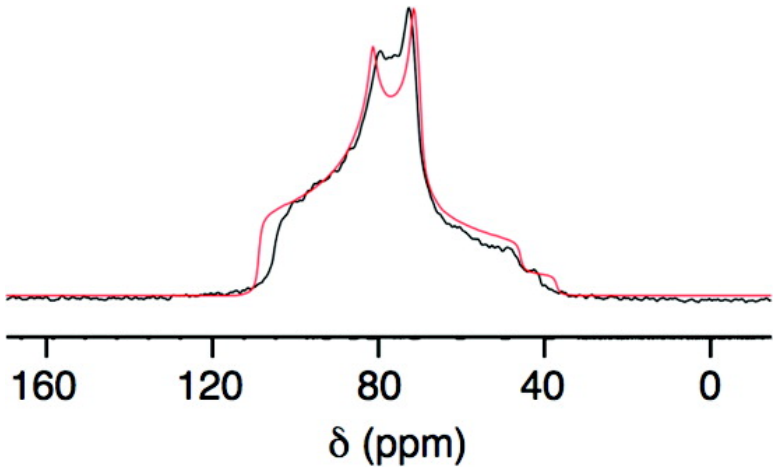

More About This Article

Additional resources and features associated with this article are available within the HTML version:

- Supporting Information
- Links to the 6 articles that cite this article, as of the time of this article download
- Access to high resolution figures
- Links to articles and content related to this article
- Copyright permission to reproduce figures and/or text from this article

View the Full Text HTML

J|A|C|S
ARTICLES
Published on Web 10/09/2007

^{17}O and ^{29}Si NMR Parameters of $MgSiO_3$ Phases from High-Resolution Solid-State NMR Spectroscopy and First-Principles Calculations

Sharon E. Ashbrook,*,† Andrew J. Berry,‡ Daniel J. Frost,§ Alan Gregorovic,|| Chris J. Pickard,⊥ Jennifer E. Readman,#,⊗ and Stephen Wimperis||

Contribution from the School of Chemistry and EaStCHEM, University of St Andrews, North Haugh, St Andrews KY16 9ST, U.K., Department of Earth Sciences and Engineering, Imperial College London, South Kensington SW7 2AZ, U.K., Bayerisches Geoinstitut, Universität Bayreuth, D-95440 Bayreuth, Germany, Department of Chemistry and WestCHEM, University of Glasgow, Glasgow G12 8QQ, U.K., School of Physics and Astronomy, University of St Andrews, North Haugh, St Andrews KY16 9SS, U.K., and Department of Chemistry, University of Exeter, Stocker Road, Exeter EX4 4QD, U.K.

Received June 18, 2007; E-mail: sema@st-andrews.ac.uk

Abstract: The ^{29}Si and ^{17}O NMR parameters of six polymorphs of $MgSiO_3$ were determined through a combination of high-resolution solid-state NMR and first-principles gauge including projector augmented wave (GIPAW) formalism calculations using periodic boundary conditions. $MgSiO_3$ is an important component of the Earth's mantle that undergoes structural changes as a function of pressure and temperature. For the lower pressure polymorphs (ortho-, clino-, and protoenstatite), all oxygen species in the ^{17}O high-resolution triple-quantum magic angle spinning (MAS) NMR spectra were resolved and assigned. These assignments differ from those tentatively suggested in previous work on the basis of empirical experimental correlations. The higher pressure polymorphs of $MgSiO_3$ (majorite, akimotoite, and perovskite) are stabilized at pressures corresponding to the Earth's transition zone and lower mantle, with perovskite being the major constituent at depths >660 km. We present the first ^{17}O NMR data for these materials and confirm previous ^{29}Si work in the literature. The use of high-resolution multiple-quantum MAS (MQMAS) and satellite-transition MAS (STMAS) experiments allows us to resolve distinct oxygen species, and full assignments are suggested. The six polymorphs exhibit a wide variety of structure types, providing an ideal opportunity to consider the variation of NMR parameters (both shielding and quadrupolar) with local structure, including changes in coordination number, local geometry (bond distances and angles), and bonding. For example, we find that, although there is a general correlation of increasing ^{17}O chemical shift with increasing Si−O bond length, the shift observed also depends upon the exact coordination environment.

Introduction

The Earth's mantle is characterized by a number of seismic discontinuities. These define the upper mantle (to a depth of 410 km), the transition zone (410−660 km), and the lower mantle (660 km to the mantle−core boundary at 2900 km). The boundaries correspond to the structural phase changes of the principal mineralogical component of the mantle, $(Mg,Fe)_2SiO_4$. With increasing pressure, olivine or forsterite (the Fe-free component; α-Mg_2SiO_4) converts to wadsleyite (β-Mg_2SiO_4; at 410 km), wadsleyite converts to ringwoodite (γ-Mg_2SiO_4; in the transition zone), and ringwoodite disproportionates to $MgSiO_3$ (perovskite) and MgO (at 660 km).[1]

After Mg_2SiO_4, the next most abundant component of the mantle is $MgSiO_3$. In the upper mantle this takes the form of pyroxenes, which have both monoclinic (clinoenstatite) and orthorhombic (protoenstatite and orthoenstatite) polymorphs. In the transition zone, the pyroxenes dissolve into a garnet phase, forming a solid solution between pyrope ($Mg_3Al_2Si_3O_{12}$) and majorite ($Mg_3(Mg,Si)Si_3O_{12}$). With increasing pressure, majorite transforms to perovskite, which is also formed from the breakdown of ringwoodite. This perovskite is the dominant mineral of the lower mantle. At the base of the transition zone, a further $MgSiO_3$ polymorph with the ilmenite structure, called akimotoite, may also occur. The triple point of majorite, perovskite, and akimotoite is 20.0 GPa and 1920 °C. From this point, in general terms, the stability field of majorite occurs at higher temperatures and that of akimotoite at lower temperatures, while perovskite is stabilized at higher pressures.[2]

† School of Chemistry and EaStCHEM, University of St Andrews.
‡ Imperial College London.
§ Universität Bayreuth.
|| University of Glasgow.
⊥ School of Physics and Astronomy, University of St Andrews.
University of Exeter.
⊗ Present address: School of Chemistry, University of Birmingham, Edgbaston, Birmingham B15 2TT, UK.

(1) Ringwood, A. E. *Composition and Petrology of the Earth's Mantle*; McGraw-Hill: New York, 1975.
(2) Hirose, K.; Komabayashi, T.; Murakami, M.; Funakoshi, K. *Geophys. Res. Lett.* **2001**, *28*, 4351.

The structure of these $MgSiO_3$ minerals is of interest because of their abundance and hence importance in understanding the physical properties of the mantle. Of particular interest is the storage in the mantle of an amount of water equivalent to at least that present currently on the surface of the Earth.[3,4] This water, or more correctly H, is thought to be stored at defect sites in nominally anhydrous minerals, such as the polymorphs of $MgSiO_3$ and Mg_2SiO_4, and may drastically affect geophysical behavior. As a result, the crystal chemistry of mantle phases, their possible hydration sites, and their water capacity has received much recent attention.[5]

In this work, we use a combination of high-resolution ^{17}O and ^{29}Si solid-state nuclear magnetic resonance (NMR) and first-principles calculations to probe the local structure in the $MgSiO_3$ polymorphs ortho-, proto-, and clinoenstatite, majorite, akimotoite, and perovskite. NMR is an excellent probe of both structure and dynamics in crystalline and disordered materials, providing information without any requirement for long-range order. As ^{29}Si has a spin quantum number $I = {}^1/_2$, high-resolution NMR spectra (free from anisotropic interactions, such as dipolar coupling and chemical shift anisotropy, which broaden spectra in the solid state) are available using conventional magic angle spinning (MAS). In contrast, ^{17}O has a spin quantum number of $I = {}^5/_2$, and the spectra are broadened by the second-order quadrupolar interaction, which cannot be removed by MAS. In order to achieve the resolution required to separate distinct species, more sophisticated approaches, such as the two-dimensional multiple-quantum MAS (MQMAS)[6] and satellite-transition MAS (STMAS)[7,8] experiments, are required. Although MQMAS is a commonly used experiment, it suffers from poor sensitivity, arising from the inefficiency of the filtration through multiple-quantum coherences. In contrast, the sensitivity of STMAS is usually much greater (often by a factor of 2−8), although the approach is technically more difficult to implement.

While both ^{17}O and ^{29}Si NMR spectra of the enstatite polymorphs (which can be synthesized at relatively low pressures) are available in the literature,[9−14] there exists limited ^{29}Si data[15−17] and no ^{17}O data for the high-pressure polymorphs. The synthesis of these phases requires the use of a multi-anvil apparatus, and in many cases only small amounts of material can be produced, significantly limiting the NMR sensitivity. However, recent work has demonstrated that the study of such quantities by NMR is possible, with STMAS being used to resolve and suggest assignments for the oxygen species in the high-pressure polymorphs of Mg_2SiO_4, wadsleyite and ringwoodite.[18,19] Only 5−10 mg of material was available, but isotopic enrichment (to ∼35%) of ^{17}O (natural abundance ∼0.037%) was used. The NMR sensitivity may be further improved by using a larger multi-anvil apparatus (able to produce up to 50 mg of material) and also by increasing the levels of isotopic enrichment (which involves considerable expense). In the current work, we employ 75% enrichment of ^{17}O.

Despite these increases in sensitivity, both spectral analysis and the extraction of accurate shielding and quadrupolar parameters remain significant challenges. These parameters (and their variation with structure, e.g., bond distances and angles) provide a vast amount of information, yielding insight into materials where the structure may be less well known. The use of ab initio or first-principles calculations to complement experimental measurements and aid the interpretation and, in particular, assignment of NMR spectra is becoming increasingly common, owing to improvements in computing hardware and software development. For solids, the recent advent of the gauge including projector augmented wave (GIPAW)[20] formalism, implemented within CASTEP,[21] a planewave, pseudopotential code that exploits the periodic nature of many solids, has allowed the calculation of both shielding and quadrupolar tensors for a variety of nuclei in a range of materials. We have recently demonstrated the use of this approach for the calculation of the shielding and quadrupolar tensors in the Mg_2SiO_4 polymorphs forsterite, wadsleyite, and ringwoodite.[22] The calculations enabled the unambiguous assignment of the NMR spectra and confirmed parameters that had been difficult to determine experimentally. In particular, it was shown that some of the quadrupolar coupling constants (C_Q) for "nonbridging" oxygen species (i.e., those bonded only to a single Si, in contrast to the "bridging" Si−O−Si species) were significantly higher than those that would be predicted on the basis of literature results. In this work, we have utilized high-resolution ^{17}O and ^{29}Si solid-state NMR, alongside first-principles calculations, to study the local environment in the $MgSiO_3$ polymorphs. These calculations facilitate spectral assignment and interpretation where sensitivity may be a limiting factor and provide a more detailed insight into the general dependence of both shielding and quadrupolar parameters upon local structure in the silicate materials that constitute the Earth's mantle.

Experimental Methods

Sample Preparation. ^{17}O-enriched SiO_2 and $Mg(OH)_2$ were prepared from the reaction of $H_2{}^{17}O$ (75%) with $SiCl_4$ and Mg_3N_2, respectively.[23] These were mixed in the stoichiometry of $MgSiO_3$, pressed into a pellet, and fired under N_2 at 600 °C (1 h). Orthoenstatite was synthesized from this mix at 1.0 GPa and 1100 °C using a piston-

(3) Kohlstedt, D. L.; Keppler, H.; Rubie, D. C. *Contrib. Mineral. Petrol.* **1996**, *123*, 345.
(4) Bolfan-Casanova, N.; Keppler, H.; Rubie, D. C. *Earth Planet. Sci. Lett.* **2000**, *182*, 209.
(5) Smyth, J. R. In *Water in Nominally Anhydrous Minerals*; Keppler, H., Smyth, J. R., Eds.; Reviews in Mineralogy and Geochemistry 62; Mineralogical Society of America: Chantilly, VA, 2006; p 85.
(6) Frydman, L.; Harwood, J. S. *J. Am. Chem. Soc.* **1995**, *117*, 5367.
(7) Gan, Z. *J. Am. Chem. Soc.* **2000**, *122*, 3242.
(8) Ashbrook, S. E.; Wimperis, S. *Prog. Nucl. Magn. Reson. Spectrosc.* **2004**, *45*, 53.
(9) Smith, K. A.; Kirkpatrick, R. J.; Oldfield, E.; Henderson, D. *Am. Mineral.* **1983**, *68*, 1206.
(10) Magi, M.; Lippmaa, E.; Samoson, A.; Engelhardt, G.; Grimmer, A. R. *J. Phys. Chem.* **1984**, *88*, 1518.
(11) Timken, H. K. C.; Schramm, S.; Kirkpatrick, R. J.; Oldfield, E. *J. Phys. Chem.* **1987**, *91*, 1054.
(12) Mueller, K. T.; Wu, Y.; Chmelka, B. F.; Stebbins, J.; Pines, A. *J. Am. Chem. Soc.* **1991**, *113*, 32.
(13) Mueller. K. T.; Baltisberger, J. H.; Wooten, E. W.; Pines, A. *J. Phys. Chem.* **1992**, *96*, 7001.
(14) Ashbrook, S. E.; Berry, A. J.; Wimperis, S. *J. Phys. Chem. B* **2002**, *106*, 773.
(15) Stebbins, J. F.; Kanzaki, M. *Science* **1991**, *251*, 294.
(16) Kirkpatrick, R. J.; Howell, D.; Phillips, B.; Cong, X. D.; Ito, E.; Navrotsky, A. *Am. Mineral.* **1991**, *76*, 673.
(17) Phillips, B. L.; Burnley, P. C.; Worminghaus, K.; Navrotsky, A. *Phys. Chem. Mineral.* **1997**, *24*, 179.
(18) Ashbrook, S. E.; Berry, A. J.; Hibberson, W. O.; Steuernagel, S.; Wimperis, S. *J. Am. Chem. Soc.* **2003**, *125*, 11824.
(19) Ashbrook, S. E.; Berry, A. J.; Hibberson, W. O.; Steuernagel, S.; Wimperis, S. *Am. Mineral.* **2005**, *90*, 1861.
(20) Pickard, C. J.; Mauri, F. *Phys. Rev. B* **2001**, *63*, 245101.
(21) Segall, M. D.; Lindan, P. J. D.; Probert, M. J.; Pickard, C. J.; Hasnip, P. J.; Clark, S. J.; Payne, M. C. *J. Phys.: Condens. Matter* **2002**, *14*, 2717.
(22) Ashbrook, S. E.; Le Polles, L.; Pickard, C. J.; Berry, A. J.; Wimperis, S.; Farnan, I. *Phys. Chem. Chem. Phys.* **2007**, *9*, 1587.
(23) Ashbrook, S. E.; Berry, A. J.; Wimperis, S. *Am. Mineral.* **1999**, *84*, 1191.

cylinder apparatus. In two experiments, approximately 250 mg of material was produced. The orthoenstatite was then converted to akimotoite at 19.5 GPa and 1400 °C (2 h), majorite at 19.5 GPa and 1950 °C (30 min), and perovskite at 23 GPa and 1650 °C (20 min).[3,24,25] The perovskite was synthesized in a Pt capsule using a MA8-type multi-anvil[26] and an 8/3 assembly (octahedral edge-length/truncation edge-length, in mm). Akimotoite and majorite were synthesized with an 18/8 assembly (Re capsule) in a split-cylinder multi-anvil (5000-tonne hydraulic press). This large-volume apparatus can allow up to 50 mg of material to be prepared in a single experiment at transition zone pressures. Further details of the press and assembly are given in ref 27. All compounds were determined to be essentially single phase by either X-ray diffraction or Raman spectroscopy. The orthopyroxene sample contained a small amount of quartz (2−3 wt %), resulting in the identification of stishovite in the sample of akimotoite.

NMR Spectroscopy. NMR spectra were obtained using either a Bruker 400 Avance I or 600 Avance III spectrometer, equipped with a wide-bore 9.4 or 14.1 T magnet, respectively. Spectra were recorded at Larmor frequencies of 79.3 MHz for ^{29}Si and 54.3 MHz (9.4 T) or 81.4 MHz (14.1 T) for ^{17}O. Samples (142 mg for orthoenstatite, 19 mg for akimotoite, 16.5 mg for majorite, and 3 mg for perovskite) were packed into conventional 2.5- or 4-mm rotors, and MAS rates between 10 and 25 kHz were employed. Orthoenstatite was powdered for NMR experiments, while the other compounds were studied as solid pellets, packed in the center of the rotor, and surrounded by an inert material (e.g., $RbNO_3$ or Bi_2O_3) of similar density to ensure stable spinning. Recycle intervals were optimized experimentally (and were typically 1−3 s for ^{17}O and ∼60 s for ^{29}Si); in addition, a number of "dummy" transients were also acquired. Two-dimensional triple-quantum and satellite-transition MAS experiments were recorded using phase-modulated split-t_1 pulse sequences.[8,28,29] In many cases, a double-quantum filter (DQF) was used in STMAS experiments to ensure the removal of the undesirable autocorrelation diagonal.[30] In all STMAS experiments, the rotor angle was adjusted prior to the experiment (to within an estimated accuracy of ±0.002°) using $RbNO_3$ or a similar material.[8,31] The ppm scales are referenced to H_2O (^{17}O) and TMS (^{29}Si). Further experimental details are given in the figure captions.

Calculations. Calculations were carried out with the CASTEP[21] density functional theory (DFT) code using the GIPAW[20] algorithm, which allows the reconstruction of the all-electron wave function in the presence of a magnetic field. The generalized gradient approximation (GGA) PBE[32] functional was employed, and the core−valence interactions were described by ultrasoft pseudopotentials.[33] For ^{17}O, the 2s and 2p orbitals were considered as valence states with a core radius of 1.3 Å, while for ^{29}Si, a core radius of 1.8 Å was used with 3s and 3p valence orbitals. Integrals over the Brillouin zone were performed using a Monkhorst−Pack grid with a k-point spacing of 0.04 $Å^{-1}$ or, in some cases, 0.05 $Å^{-1}$.[34] Wave functions were expanded in planewaves with a kinetic energy smaller than the cutoff energy, typically ∼700 eV. All calculations were converged as far as possible with respect to both k-point spacing and cutoff energy. Repeated calculations yielded the same results to within two decimal places.

Structural parameters (the unit cell and all atomic positions) were obtained from experimental diffraction studies in the literature, with corresponding references given in the text. The crystalline structure was reproduced from these parameters by the use of periodic boundary conditions. The numbers of atoms in the unit cell were 80 (orthoenstatite), 40 (clino- and protoenstatite), 30 (akimotoite), 160 (majorite), and 20 (perovskite). In most cases, the forces observed on the atoms were small, indicating that the structures chosen were very nearly relaxed. Where necessary, geometry optimization was performed within the CASTEP program, and both the lattice parameters and atomic coordinates were allowed to vary. After optimization, forces less than ∼50 meV $Å^{-1}$ were observed. In most cases, optimization produced very little change in the NMR parameters, with any significant changes described in detail in the text. No additional rescaling to account for any density functional error in bond lengths was performed. Calculations were performed on the EaStCHEM Research Computing Facility, which consists of 98 AMD Opteron processing cores connected by Infinipath high-speed interconnects. Calculation times typically ranged from 36 to 1200 processor hours.

The calculations produce the absolute shielding tensor (σ) and the electric field gradient (EFG) tensor (**V**) in the crystal reference frame, with diagonalization of these tensors providing the principal components or eigenvalues. The isotropic chemical shift, δ_{iso}, can be obtained from the isotropic chemical shielding, σ_{iso}:

$$\sigma_{iso} = {}^1/_3\,\mathrm{Tr}\{\sigma\} \quad (1)$$

$$\delta_{iso} = -(\sigma_{iso} - \sigma_{ref}) \quad (2)$$

where σ_{ref} is a reference isotropic shielding. Experimentally, this is obtained by measuring the chemical shift of an external reference sample. For the calculations, chemical shieldings were referenced to previous work on Mg_2SiO_4 (forsterite), resulting in σ_{ref} values of 255.0 and 312.7 ppm for ^{17}O and ^{29}Si, respectively. This allows direct comparison with our previous results and reduces the effects of any significant systematic DFT error. From the principal components of the symmetric part of the shielding tensor, the magnitude, Δ_{CS}, and asymmetry, η_{CS}, of the chemical shift anisotropy (CSA) can be calculated:

$$\Delta_{CS} = \sigma_{ZZ} - \sigma_{iso} \quad (3)$$

$$\eta_{CS} = (\sigma_{YY} - \sigma_{XX})/(\sigma_{ZZ} - \sigma_{iso}) \quad (4)$$

Here, σ_{ii} are the principal components of the symmetric shielding tensor such that $|\sigma_{ZZ} - \sigma_{iso}| \geq |\sigma_{XX} - \sigma_{iso}| \geq |\sigma_{YY} - \sigma_{iso}|$.

The quadrupolar interaction is characterized by a magnitude, C_Q, and an asymmetry, η_Q:

$$C_Q = eQV_{ZZ}/h \quad (5)$$

$$\eta_Q = (V_{XX} - V_{YY})/V_{ZZ} \quad (6)$$

where the principal components of the EFG tensor are ordered such that $|V_{ZZ}| \geq |V_{YY}| \geq |V_{XX}|$ and Q is the nuclear electric quadrupole moment. The quadrupolar product, P_Q, is then given by

$$P_Q = C_Q(1 + \eta_Q{}^2/3)^{1/2} \quad (7)$$

An experimentally determined quadrupole moment, eQ, of 25.58 mB[35] was used for ^{17}O. The sign of C_Q cannot be determined at room temperature from a simple MAS spectrum, and so absolute values of C_Q have been studied. It should be noted, however, that the calculated ^{17}O C_Q values of all oxygen species considered here are negative except for akimotoite.

(24) Ono, S.; Hatsura, E.; Ito, E.; Kanzaki, M.; Yoneda, A.; Walter, M. J. *Geophys. Res. Lett.* **2001**, *28*, 835.
(25) Kuroda, K.; Irifune, T.; Inoue, T.; Nishiyama, N.; Miyashita, M.; Funakoshi, K.; Utsumi, W. *Phys. Chem. Mineral.* **2000**, *27*, 523.
(26) Ohtani, E.; Irifune, I.; Hibberson, W. O.; Ringwood, A. E. *High-Temp. High-Press.* **1987**, *19*, 523.
(27) Frost, D. J.; Poe, B. T.; Tronnes, R. G.; Liebske, C.; Duba, A.; Rubie, D. C. *Phys. Earth. Planet. Int.* **2004**, *143/144*, 507.
(28) Brown, S. P.; Wimperis, S. *J. Magn. Reson.* **1997**, *128*, 42.
(29) Pike, K. J.; Ashbrook, S. E.; Wimperis, S. *Chem. Phys. Lett.* **2001**, *345*, 400.
(30) Kwak, H. T.; Gan, Z. *J. Magn. Reson.* **2003**, *164*, 369.
(31) Ashbrook, S. E; Wimperis, S. *J. Magn. Reson.* **2002**, *156*, 269.
(32) Perdew, J. P.; Burke, K.; Ernzerhof, M. *Phys. Rev. Lett.* **1996**, *77*, 3865.
(33) Yates, J. R.; Pickard, C. J.; Mauri, F. *Phys. Rev. B* **2007**, *76*, 024401.
(34) Monkhorst, H.; Pack, J. D. *Phys. Rev. B* **1976**, *13*, 5188.
(35) Pyykkö, P. *Mol. Phys.* **2001**, *19*, 1617.

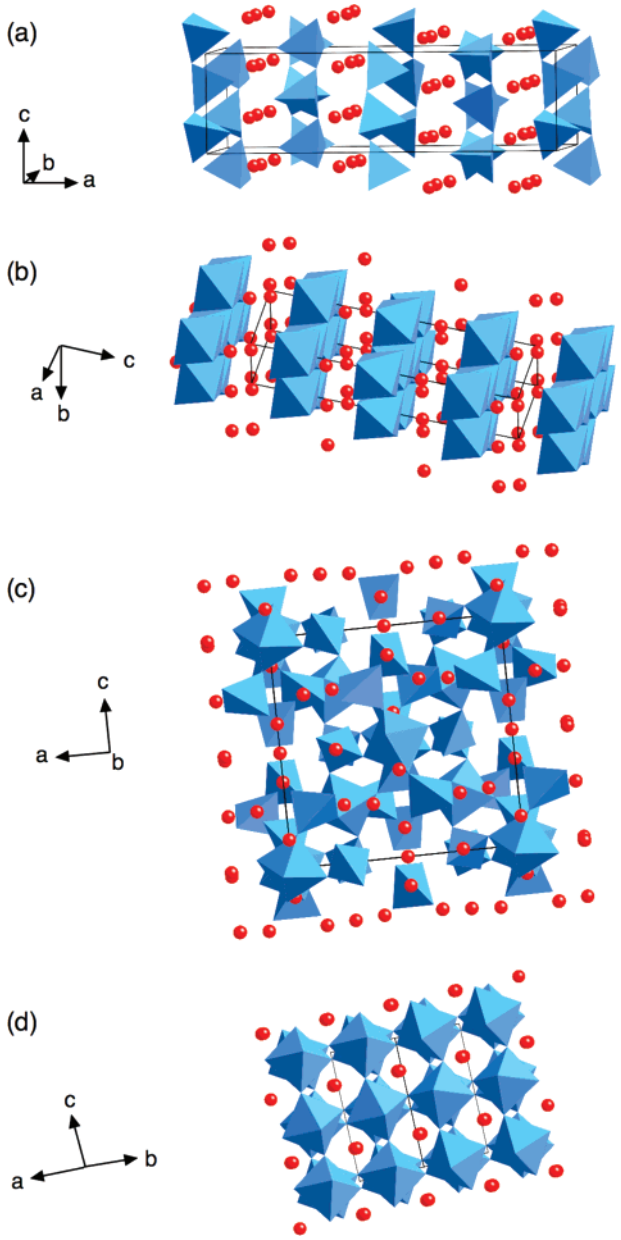

Figure 1. Structure of $MgSiO_3$ polymorphs (a) orthoenstatite, (b) akimotoite, (c) majorite, and (d) perovskite. SiO_n polyhedra are shown in blue and Mg atoms in red.

Results

I. Enstatite. The enstatite polymorphs include orthorhombic orthoenstatite (*Pbca*)[36] and protoenstatite (*Pbcn*)[37] and monoclinic clinoenstatite ($P2_1/c$).[38] All are chain silicates with corner-sharing SiO_4 tetrahedra linked by Mg^{2+} cations, as shown (for orthoenstatite) in Figure 1a. In each chain there are two nonbridging oxygen species, O1 and O2, and a bridging oxygen, O3, linking the tetrahedra. For protoenstatite, only a single type of chain is present, whereas for clinoenstatite and orthoenstatite there are two slightly different chains, producing pairs of similar O1, O2, and O3 species, and a total of six different oxygen sites. As only relatively low synthesis pressures are required, allowing large sample volumes, there have been a number of previous NMR studies of the enstatites, including both ^{29}Si and ^{17}O.[9−14] In particular, high-resolution ^{17}O MQMAS experiments were used to resolve all oxygen species for each polymorph: six for orthoenstatite and clinoenstatite and three for protoenstatite.[14] Although nonbridging and bridging oxygens could be differentiated fairly easily owing to significant differences in P_Q values (usually 2−3 and 4−6 MHz, respectively), a full spectral assignment proved more difficult, with many species possessing similar NMR parameters. Tentative assignments were suggested on the basis of a comparison with Mg_2SiO_4 (forsterite)[23] and empirical observations in the literature.[39]

Table 1. Calculated ^{29}Si NMR Parameters (Isotropic Chemical Shift, δ_{iso}; Chemical Shift Anisotropy, Δ_{CS}; and Shielding Asymmetry, η_{CS}) for the $MgSiO_3$ Polymorphs Orthoenstatite, Clinoenstatite, Protoenstatite, Akimotoite, Majorite, and Perovskite

mineral		population	type[a]	δ_{iso} (ppm)	Δ_{CS} (ppm)	η_{CS}
orthoenstatite	Si1	1	$Si^{(IV)}$ Q^2	−85.1	54.4	0.70
	Si2	1	$Si^{(IV)}$ Q^2	−82.0	55.1	0.63
clinoenstatite	Si1	1	$Si^{(IV)}$ Q^2	−85.3	54.2	0.71
	Si2	1	$Si^{(IV)}$ Q^2	−82.1	55.1	0.64
protoenstatite	Si1	1	$Si^{(IV)}$ Q^2	−88.3	49.8	0.78
(optimized)	Si1	1	$Si^{(IV)}$ Q^2	−87.4	52.1	0.74
akimotoite	Si1	1	$Si^{(VI)}$ Q^6	−178.5	−14.1	0.01
majorite	Si1	2	$Si^{(VI)}$ Q^6	−194.1	−5.2	0.09
	Si2	1	$Si^{(IV)}$ Q^0	−68.5	9.1	0.00
	Si3	1	$Si^{(IV)}$ Q^4	−93.7	13.3	0.00
	Si4	4	$Si^{(IV)}$ Q^2	−75.1	37.9	0.61
perovskite	Si1	1	$Si^{(VI)}$ Q^6	−191.5	3.6	0.59

[a] $Si^{(x)}$, x = coordination number; Q^n, n = number of bridging oxygen species.

Tables 1 and 2 give the ^{29}Si and ^{17}O NMR shielding and quadrupolar parameters for the three enstatite polymorphs, calculated from first-principles. For protoenstatite, the forces on the atoms predicted by the calculation were relatively large, and so a second calculation was performed after the geometry (atomic coordinates and unit cell dimensions) was optimized. However, this produced only small changes in the NMR parameters, as shown in Tables 1 and 2. For all three polymorphs, ^{29}Si isotropic chemical shifts of between −82 and −89 ppm were observed (Table 1), typical of the Q^2 species expected in chain silicates. (The Q^n nomenclature refers to the number of bridging oxygen species, n, to which the silicon is coordinated). Table 2 shows that, although a clear distinction is apparent between nonbridging and bridging oxygens, many species have similar ^{17}O quadrupolar and shielding parameters. From the values of δ_{iso}, C_Q, and η_Q, we can predict the δ_1 position of the corresponding resonance in a triple-quantum split-t_1 MAS experiment (or the corresponding satellite-transition split-t_1 MAS experiment), i.e., the shift in the isotropic spectrum. For ^{17}O ($I = {}^5/_2$), these are given (in ppm), using the conventions described in refs 8 and 40, by

$$\delta_1 = (17/31)\delta_{iso} + (32/93)\delta_Q \quad (8)$$

with the isotropic second-order quadrupolar shift parameter

$$\delta_Q = (75P_Q/\nu_0)^2 \quad (9)$$

(36) Sasaki, S.; Takeuchi, Y.; Fujino, K.; Akimoto, S. *Z. Kristallogr.* **1982**, *158*, 279.
(37) Murakami, T.; Takéuchi, Y.; Yamanaka, T. *Z. Kristallogr.* **1982**, *160*, 299.
(38) Ohashi, Y.; Finger, L. W. *Carnegie Inst. Washington Year Book* **1976**, *75*, 743.
(39) Ashbrook, S. E.; Berry, A. J.; Wimperis, S. *J. Am. Chem. Soc.* **2001**, *123*, 6360.

Table 2. Calculated ^{17}O NMR Parameters (Triple-Quantum/Satellite-Transition MAS Shifts, δ_1, at 9.4 T; Isotropic Chemical Shifts, δ_{iso}; Quadrupolar Products, P_Q; Quadrupolar Coupling Constants, C_Q; and Quadrupolar Asymmetries, η_Q) for the $MgSiO_3$ Polymorphs Orthoenstatite, Clinoenstatite, Protoenstatite, Akimotoite, Majorite, and Perovskite

mineral		population	type[a]	δ_1 (ppm), 9.4 T	δ_{iso} (ppm)	P_Q (MHz)[b]	C_Q (MHz)	η_Q
orthoenstatite	O11	1	nbo	28.7	41.0	3.09	3.06	0.21
	O12	1	nbo	32.1	47.8	3.01	2.96	0.30
	O21	1	nbo	37.8	57.4	3.09	3.03	0.35
	O22	1	nbo	36.1	53.4	3.22	3.03	0.61
	O31	1	bo	49.4	62.6	4.79	4.35	0.80
	O32	1	bo	60.9	74.4	5.53	5.00	0.82
clinoenstatite	O11/O1	1	nbo	28.9	41.6	3.05	3.03	0.22
	O12/O4	1	nbo	32.1	47.9	2.97	2.93	0.29
	O21/O2	1	nbo	38.3	57.6	3.19	3.05	0.54
	O22/O5	1	nbo	35.4	52.2	3.21	3.04	0.59
	O31/O3	1	bo	49.6	61.9	4.87	4.35	0.88
	O32/O6	1	bo	60.5	73.6	5.54	4.98	0.84
protoenstatite	O1	1	nbo	26.1	38.2	2.81	2.77	0.29
	O2	1	nbo	34.4	51.7	3.02	2.93	0.45
	O3	1	bo	48.6	58.9	4.98	4.81	0.47
protoenstatite	O1	1	nbo	28.4	39.7	3.05	3.03	0.23
(optimized)	O2	1	nbo	35.7	52.6	3.09	3.00	0.43
	O3	1	bo	51.9	62.0	5.14	4.90	0.48
akimotoite	O1	1	bo	71.9	111.0	3.91	3.61	0.72
majorite	O1	1	nbo	50.5	80.8	3.07	3.01	0.37
	O2	1	bo	81.8	117.4	5.14	4.91	0.54
	O3	1	bo	78.2	114.9	4.80	4.64	0.45
	O4	1	nbo	53.8	84.3	3.40	3.37	0.20
	O5	1	nbo	47.3	75.9	2.94	2.87	0.38
	O6	1	bo	80.0	110.6	5.35	5.31	0.21
perovskite	O1	1	bo	82.8	116.0	5.37	5.31	0.28
	O2	2	bo	83.0	117.0	5.33	5.32	0.12

[a] nbo = nonbridging oxygen, bo = bridging oxygen. [b] P_Q is calculated from $C_Q(1 + \eta_Q^2/3)^{1/2}$.

These are given in Table 2 for $B_0 = 9.4$ T. The values are in good agreement with those found experimentally.[14] Notably, the isotropic spectra of orthoenstatite and clinoenstatite are predicted to be very similar (as observed experimentally in ref 14), despite the significant differences in some quadrupolar asymmetry parameters. However, the results in Table 2 do not support the previously suggested assignment.[14] For example, in the case of orthoenstatite, the spectral peaks were assigned as O21, O22, O11, O12, O31, and O32 in order of increasing δ_1 shift, while Table 2 predicts that the corresponding order at 9.4 T should be O11, O12, O22, O21, O31, and O32. Given the similarity of many of the species, this disagreement is perhaps not too surprising.

In order to clarify the spectral assignment, a new sample of orthoenstatite (synthesized with an enrichment level of 75%) was studied. Figure 2 shows ^{29}Si and ^{17}O MAS NMR spectra of this material, with corresponding parameters given in Table 3. Two ^{29}Si peaks were observed at δ_{iso} values of -80.7 and -83.2 ppm (Figure 2a), in good agreement with the calculated predictions and assigned, with reference to Table 1, as Si2 and Si1, respectively. The ^{17}O MAS NMR spectrum (Figure 2b) contains a composite resonance owing to the overlap of second-order quadrupolar broadened line shapes. Figure 2c,d shows that resolution is increased in a triple-quantum MAS spectrum, with six sharp resonances observed in the isotropic dimension. The two resonances at higher δ_1, with larger quadrupolar coupling constants, were assigned to the two bridging oxygens, while the four resonances at lower δ_1 shifts correspond to nonbridging oxygens. Figure 3 shows cross sections taken parallel to δ_2 through each of the six ridge line shapes (labeled (a)−(f) in order of increasing δ_1 shift), which reveal distinct quadrupolar line shapes corresponding to a variety of η_Q values. By comparing the experimental and calculated values (Table 2), it is possible to assign the spectrum, as shown in Table 3. All four nonbridging oxygens have very similar C_Q values, but

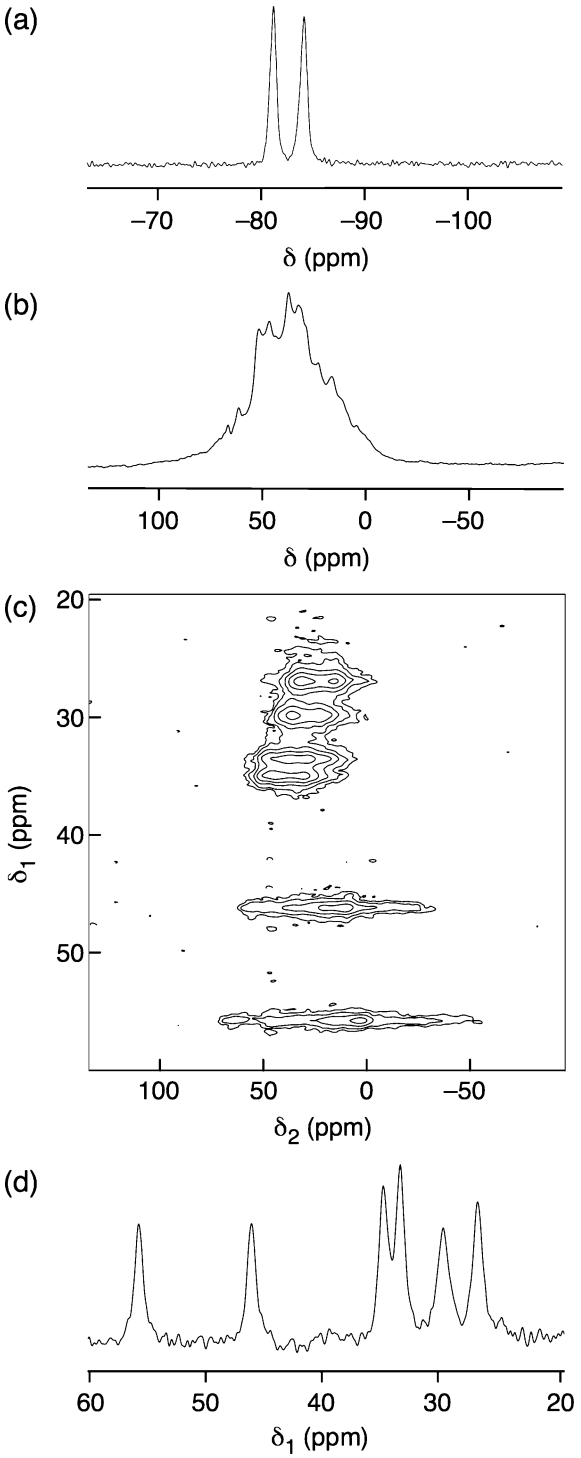

Figure 2. MAS NMR spectra of orthoenstatite. (a) ^{29}Si (79.3 MHz) MAS spectrum, (b) ^{17}O (54.3 MHz) MAS spectrum, and (c) ^{17}O (54.3 MHz) triple-quantum MAS spectrum, recorded using a rotor-synchronized phase-modulated split-t_1 experiment,[28] and (d) its isotropic projection. In (a), 64 transients were averaged with recycle interval 60 s; in (b), 240 transients were averaged with recycle interval 2 s. In (c), 384 transients were averaged for each of 256 t_1 increments of 258.33 μs, with recycle interval 2 s. In each case, the MAS rate was 10 kHz.

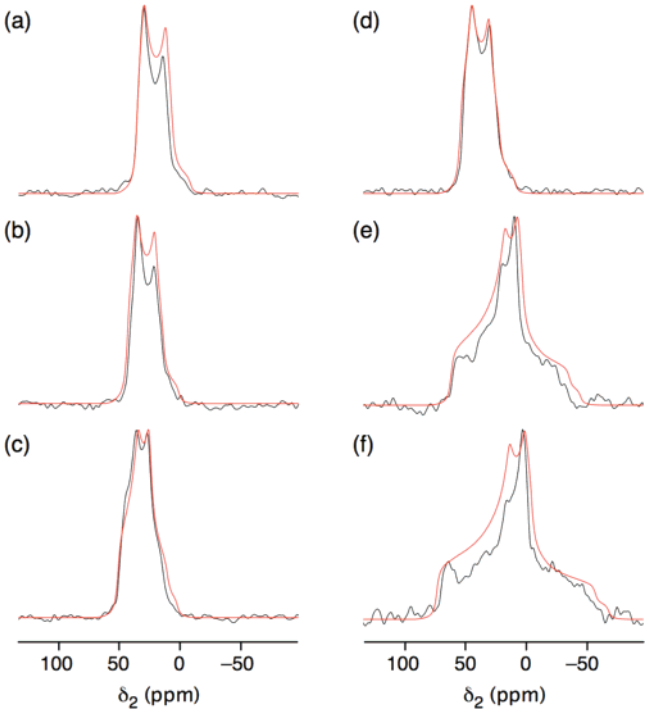

Figure 3. Cross sections, extracted parallel to δ_2, from the triple-quantum MAS spectrum of orthoenstatite in Figure 2c for δ_1 values of (a) 28, (b) 31, (c) 34, (d) 36, (e) 47, and (f) 57 ppm. Also shown (in red) are "first-principles" line shapes simulated using the parameters in Table 2.

Table 3. Experimental ^{29}Si and ^{17}O NMR Parameters (Triple-Quantum MAS Shifts, δ_1, at 9.4 T; Isotropic Chemical Shifts, δ_{iso}; Quadrupolar Products, P_Q; Quadrupolar Coupling Constants, C_Q; and Quadrupolar Asymmetries, η_Q), Extracted from the Spectra in Figures 2 and 3, and Suggested Assignments for Orthoenstatite

δ_1 (ppm), 9.4 T	δ_{iso} (ppm)	P_Q (MHz)	C_Q (MHz)	η_Q	assignment
28 (1)	41 (1)	2.9 (1)	2.9 (1)	0.19 (5)	O11
31 (1)	46 (1)	2.9 (1)	2.8 (1)	0.29 (5)	O12
34 (1)	52 (1)	3.1 (1)	2.9 (1)	0.53 (5)	O22
36 (1)	56 (1)	2.9 (1)	2.9 (1)	0.29 (5)	O21
47 (1)	60 (2)	4.6 (2)	4.2 (1)	0.78 (5)	O31
57 (1)	70 (2)	5.3 (2)	4.8 (1)	0.80 (5)	O32
	−80.7 (3)				Si2
	−83.2 (3)				Si1

differences in chemical shift enable the assignment of the peaks at δ_1 shifts of 28 and 31 ppm to O11 and O12, respectively. The peaks with δ_1 shifts of 34 and 36 ppm can be assigned to O22 and O21, on the basis of both chemical shift arguments and the distinctly different η_Q value of O22, as seen from the differences in line shape between Figure 3c and Figure 3a,b,d. The two bridging oxygens can also be identified (as O31 and O32 in order of increasing shift), with the C_Q value of O32 being significantly larger than that of O31. (It should be noted that these broader line shapes appear somewhat distorted as a result of the nonuniform excitation that is often be a problem in MQMAS.) Also shown in Figure 3 (red) are the corresponding line shapes simulated using the parameters determined by the first-principles calculations given in Table 2. These demonstrate the excellent agreement between the calculations and experiment and provide confidence in the new spectral assignment.

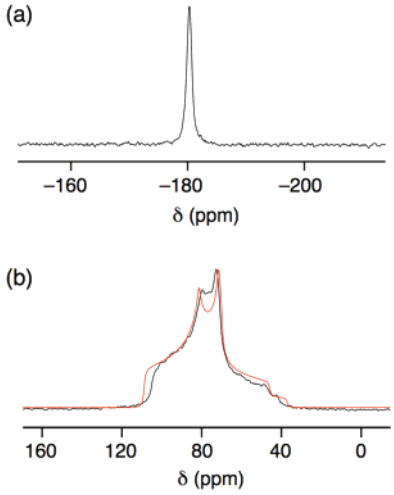

Figure 4. (a) ^{29}Si (79.3 MHz) and (b) ^{17}O (54.3 MHz) MAS NMR spectra of akimotoite. (a) 1024 and (b) 3600 transients were averaged with recycle intervals (a) 60 s and (b) 1 s. The MAS rate was 10 kHz in each case. Also shown in (b) (in red) is the "first-principles" line shape simulated using the parameters in Table 2.

Table 4. Experimental ^{29}Si and ^{17}O NMR Parameters (Isotropic Chemical Shifts, δ_{iso}; Quadrupolar Products, P_Q; Quadrupolar Coupling Constants, C_Q; and Quadrupolar Asymmetries, η_Q) for Akimotoite, Extracted from the Spectra in Figure 4

	δ_{iso} (ppm)	P_Q (MHz)	C_Q (MHz)	η_Q
O	106 (1)	3.7 (1)	3.4 (1)	0.78 (5)
Si	−180.3 (3)			

II. Akimotoite. Akimotoite has the ilmenite structure ($R\bar{3}$) and consists of layers of edge-sharing SiO_6 octahedra,[41] as shown in Figure 1b, with single oxygen and silicon species. Figure 4 shows conventional ^{29}Si and ^{17}O MAS NMR spectra of akimotoite, recorded at $B_0 = 9.4$ T. The ^{29}Si NMR spectrum (Figure 4a) reveals a single peak at −180 ppm, typical of six-coordinate ($Si^{(VI)}$) silicon, which provides no obvious evidence for any cation (i.e., $Si^{(VI)}$ and $Mg^{(VI)}$) disorder.[15] This is in agreement with the only literature work on akimotoite, where material enriched to 95% in ^{29}Si was studied.[15] The ^{17}O MAS NMR spectrum (Figure 4b) exhibits a single second-order quadrupolar broadened line shape that can be well fitted using values of $C_Q = 3.4$ MHz and $\eta_Q = 0.78$ (Table 4). The observed C_Q value is perhaps lower than might be expected for bridging oxygen species, which typically vary between 4 and 6 MHz. Calculated ^{29}Si and ^{17}O NMR parameters for akimotoite are given in Tables 1 and 2, and are in good agreement with the experimental data. Notably, a low C_Q value of 3.6 MHz is also obtained from our first-principles calculations. The agreement is also demonstrated in Figure 4b, where a line shape (shown in red) simulated using the calculated parameters in Table 2 is compared with the experimental data.

III. Majorite. Majorite has a garnet structure (Figure 1c), with space group $I41/a$ and a complex unit cell containing 160 atoms.[42] As shown in Figure 1c, both SiO_6 and SiO_4 polyhedra are present, linked by shared vertices. The structure contains

(40) Pike, K. J.; Malde, R. P.; Ashbrook, S. E.; McManus, J.; Wimperis, S. *Solid State Nucl. Magn. Reson.* **2000**, *16*, 203.
(41) Wechsler, B. A.; Prewitt, C. T. *Am. Mineral.* **1984**, *69*, 754.
(42) Hazen, R. M.; Downs, R. T.; Finger, L. W.; Conrad, P. G.; Gasparik, T. *Am. Mineral.* **1994**, *79*, 581.

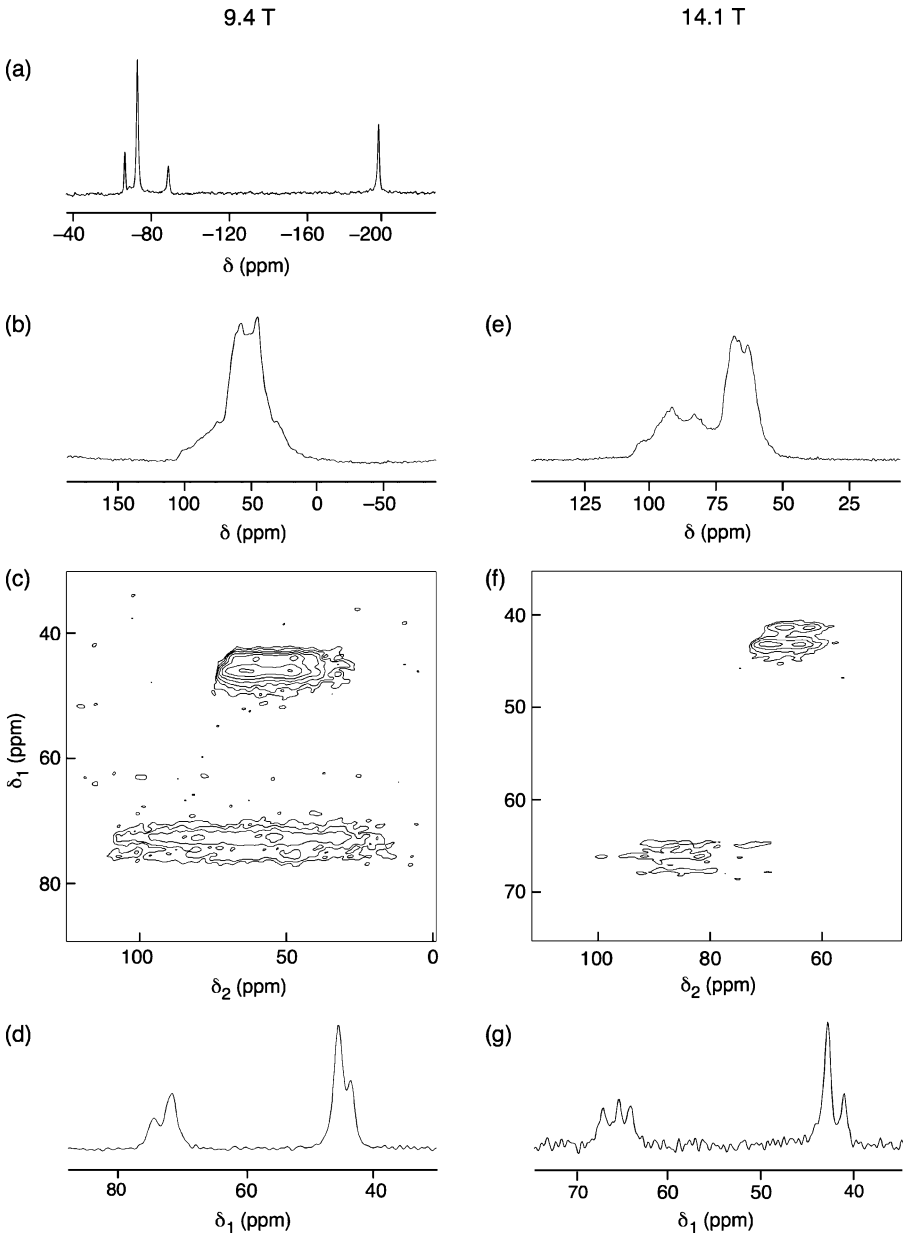

Figure 5. MAS NMR spectra of majorite. (a) ^{29}Si (79.3 MHz) MAS spectrum, (b) ^{17}O (54.3 MHz) MAS spectrum, (c) ^{17}O (54.3 MHz) satellite-transition MAS NMR spectrum, recorded using a double-quantum-filtered[30] rotor-synchronized phase-modulated split-t_1 experiment,[8] and (d) its isotropic projection, (e) ^{17}O (81.4 MHz) MAS spectrum, (f) ^{17}O (81.4 MHz) multiple-quantum MAS spectrum, recorded using a rotor-synchronized phase-modulated split-t_1 experiment,[28] and (g) its isotropic projection. (a) 1024, (b) 1200, and (e) 3600 transients were averaged with recycle intervals (a) 1 s, (b) 60 s, and (e) 2 s. In (c), 512 transients were averaged for each of 128 t_1 increments of 258.3 μs, with recycle interval 3 s, while in (f), 192 transients were averaged for each of 109 t_1 increments of 126.7 μs, with a recycle interval of 3 s. The MAS rates were (a−d) 10 kHz and (e−g) 12.5 kHz.

four different silicon species (one octahedral and three tetrahedral, with relative populations of 2:1:1:4) and six oxygen species (three bridging and three nonbridging). Figure 5a shows a ^{29}Si MAS NMR spectrum of majorite, which exhibits four distinct resonances, with intensity ratios 2:1:4:1 in order of increasing δ, and chemical shifts as detailed in Table 5. One resonance (with $\delta_{iso} = -197.1$ ppm) is typical of octahedrally coordinated silicon, while the remaining three have chemical shifts characteristic of four-coordinated species.[15] These results are in good agreement with ^{29}Si NMR data for majorite from the literature,[15] where four similar peaks were assigned to a majorite component in a mixture of high-pressure phases.

The ^{17}O (54.3 MHz) MAS NMR spectrum of majorite is shown in Figure 5b and reveals a complex line shape, resulting from the overlap of the quadrupolar broadened lines from the six different oxygen species. The DQF-STMAS spectrum in Figure 5c, and its isotropic projection in Figure 5d, provide a considerable increase in resolution, although only four sharp resonances are observed. (The MQMAS spectrum (not shown) is similar but with a lower signal-to-noise ratio.) From the chemical shifts and quadrupolar parameters (extracted from the δ_1, δ_2 position of each ridge), these four peaks appear to fall into two distinct groups: bridging (δ_1 between 70 and 80 ppm) and nonbridging (δ_1 between 40 and 50 ppm) oxygens. Given the relative intensities of the resonances in the spectrum (1:2 for both the two bridging and the two nonbridging oxygen resonances), it is tempting to suggest that all six oxygen species are present, with coincidental overlap of some of the isotropic

Table 5. Experimental ^{29}Si and ^{17}O NMR Parameters (Triple-Quantum/Satellite-Transition MAS Shifts, δ_1, at 9.4 and 14.1 T; Isotropic Chemical Shifts, δ_{iso}; Quadrupolar Products, P_Q; Quadrupolar Coupling Constants, C_Q; and Quadrupolar Asymmetries, η_Q), Extracted from the Spectra in Figures 5 and 6, and Suggested Assignments for Majorite

	δ_1 (ppm)	δ_{iso} (ppm)	P_Q (MHz)	C_Q (MHz)	η_Q	assignment
O (9.4 T)	43 (1)	69 (1)	3.0 (1)	2.9 (1)	0.33 (5)	O5
	45 (1)	72 (2)	3.1 (2)	3.0 (2)	0.3 (1)	O1+O4
	73 (1)	104 (2)	4.9 (2)			O3+O6
	76 (1)	110 (1)	4.9 (1)	4.8 (2)	0.54 (5)	O2
O (14.1 T)	41 (1)	70 (1)	2.9 (1)	2.8 (1)	0.33 (5)	O5
	43 (1)	73 (2)	3.0 (2)	3.0 (2)	0.24 (5)	O1+O4
	64 (1)	103 (1)	4.8 (1)	4.8 (1)	0.0 (1)	O6
	66 (1)	108 (1)	4.6 (1)	4.4 (1)	0.46 (5)	O3
	68 (1)	110 (1)	5.0 (1)	4.8 (1)	0.53 (5)	O2
Si		−197.1 (3)				Si1
		−90.5 (3)				Si3
		−73.9 (3)				Si4
		−67.5 (3)				Si2

resonances. The difference in relative intensities between the two types of oxygen results from nonuniform efficiency of the experiment as C_Q increases. The presence of six species appears to be confirmed by the ^{17}O (81.4 MHz) spectra in Figure 5e−g. At this higher B_0 field strength, the three bridging sites can be resolved by MQMAS and are clearly seen in the isotropic projection in Figure 5g. However, two of the three nonbridging oxygen resonances remain overlapped. Parameters extracted from these spectra are given in Table 5. Cross sections, extracted parallel to δ_2, from the 9.4 T spectrum in Figure 5c are shown in Figure 6. Those extracted for $\delta_1 = 43$ and 76 ppm (Figure 6a,d, respectively) reveal characteristic quadrupolar line shapes which can be fitted with C_Q, η_Q, and δ_{iso} as shown in Table 5. The line shape with $\delta_1 = 73$ ppm (Figure 6c) contains a complex resonance, fitted reasonably well by the overlap of two distinct line shapes. The final cross section in Figure 6b cannot be easily decomposed into two line shapes, probably owing to the similarity of the two species.

Tables 1 and 2 show the ^{29}Si and ^{17}O NMR parameters for majorite calculated from first-principles. Owing to the large number of atoms in the unit cell, it was not possible to perform the calculation with the same level of accuracy as previous calculations, and a *k*-point spacing of 0.05 Å^{-1} (rather than 0.04 Å^{-1}) was used. Although it appears that the relative shieldings are reasonably converged at this level of accuracy, it is possible that this is not true for the absolute shieldings. In addition, although the forces on the structure were reasonably high (up to 1 eV/Å), the large unit cell size also prevented optimization of the geometry. Nevertheless, the results obtained yield insight into the interpretation and assignment of the experimental spectra.

The ^{29}Si chemical shifts shown in Table 1 are in good agreement with the experimental results and allow the resonances to be identified as Si1, Si3, Si4, and Si2, in order of increasing δ_{iso}. This confirms the suggested literature assignment based on the shift ranges for six- and four-coordinate silicon and the empirical observation of increasing δ_{iso} as *n* increases, i.e., $\delta_{iso}(Q^0) < \delta_{iso}(Q^2) < \delta_{iso}(Q^4)$.[15] It was noted in this previous work that these simple considerations of the effect of neighboring cations predict three equally spaced resonances, in contrast to the experimental observation. The unequal separation of the

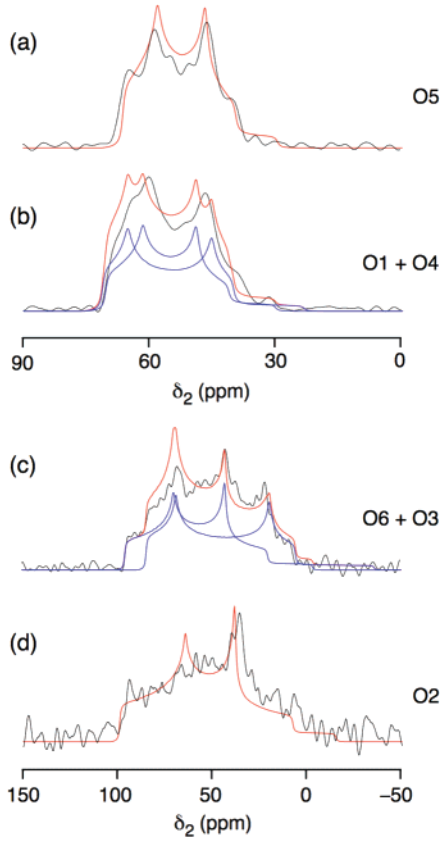

Figure 6. Cross sections, extracted parallel to δ_2, from the ^{17}O (54.3 MHz) DQF-STMAS spectrum of majorite in Figure 5c at δ_1 values of (a) 43, (b) 45, (c) 73, and (d) 76 ppm. Also shown are "first-principles" line shapes ($B_0 = 9.4$ T), simulated using the parameters in Table 2, with the full line shapes (red) decomposed into their constituent parts (blue).

three resonances is, however, reproduced by the calculated results in Table 1. The ^{17}O NMR parameters in Table 2 reveal three similar nonbridging oxygen species and three similar bridging oxygens. Although the calculations do not predict the exact overlap of any species, comparison with the experimental parameters in Table 5 allows the majority of the spectral resonances to be assigned. For the bridging oxygens, the resonance with the highest δ_1 shift at $B_0 = 9.4$ T can be assigned to O2, while that at the lower shift results from a combination of O3 and O6. For the nonbridging oxygens, the ridge with the lowest δ_1 shift appears to result from O5, while we then assume that the remaining resonance results from the overlap of O1 and O4. Similarly, at 14.1 T, resonances can be assigned as O5, O1 + O4, O6, O3, and O2 in order of increasing δ_1. Calculated ^{17}O (54.2 MHz) MAS line shapes (using the parameters shown in Table 2) for the six species in majorite are also shown in Figure 6.

IV. Perovskite. The perovskite structure consists of a framework of corner-sharing SiO_6 octahedra with Mg atoms occupying the "A" sites between the octahedra, as shown in Figure 1d. The SiO_6 octahedra are tilted, reducing the symmetry from cubic to orthorhombic (*Pbnm*) and resulting in a single silicon species but two types of bridging oxygens.[43] Figure 7a shows a ^{29}Si (79.3 MHz) MAS NMR spectrum of perovskite, containing a fairly broad resonance at −193.0 ppm (as shown in Table 6). This is in good agreement with the only literature

(43) Brown, G. E. Ph.D. thesis, Virginia Polytechnic Institute and State University, 1970.

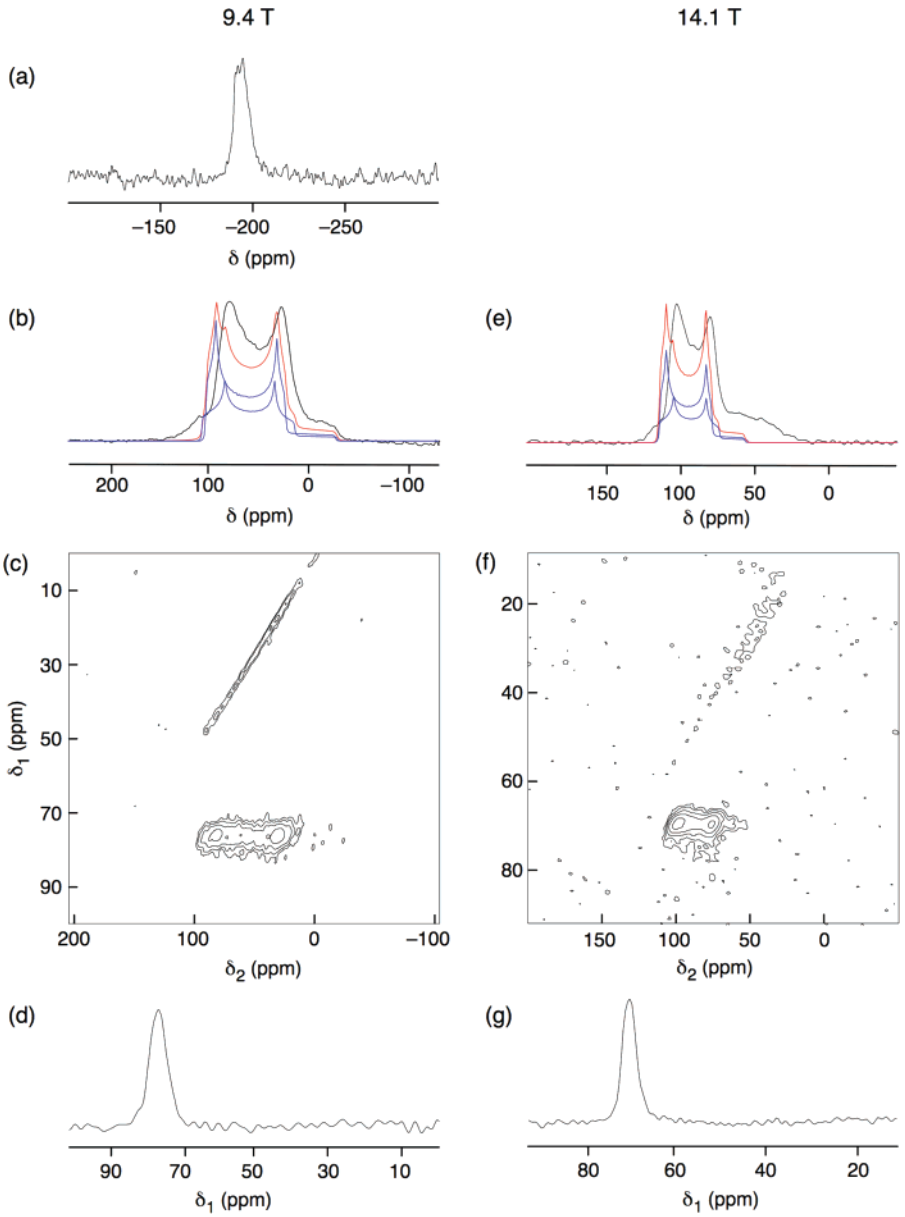

Figure 7. MAS NMR spectra of perovskite. (a) ^{29}Si (79.3 MHz) MAS spectrum, (b) ^{17}O (54.3 MHz) MAS spectrum, (c) ^{17}O (54.3 MHz) STMAS spectrum, recorded using a rotor-synchronized phase-modulated split-t_1 experiment,[8] and (d) its isotropic projection, (e) ^{17}O (81.4 MHz) MAS spectrum, (f) ^{17}O (81.4 MHz) STMAS spectrum, recorded using a double-quantum-filtered[30] rotor-synchronized phase-modulated split-t_1 experiment,[8] and (g) its isotropic projection. (a) 13 600, (b) 28 000, and (d) 2400 transients were averaged with recycle intervals (a) 30 s, (b) 2 s, and (d) 3 s. In (c), 1504 transients were averaged for each of 165 t_1 increments of 64.6 μs, with recycle interval 2 s. In (e), 768 transients were averaged for each of 107 t_1 increments of 51.6 μs, with recycle interval 2 s. The MAS rates were (a−d) 20 kHz and (e−g) 25 kHz. In (b) and (e), "first-principles" line shapes, simulated using the parameters obtained from first-principles calculations given in Table 2, are also shown, with the full line shapes (red) decomposed into their constituent parts (blue).

Table 6. Experimental ^{29}Si and ^{17}O NMR Parameters (Satellite-Transition MAS Shifts, δ_1, at 9.4 T; Isotropic Chemical Shifts, δ_{iso}; Quadrupolar Products, P_Q; Quadrupolar Coupling Constants, C_Q; and Quadrupolar Asymmetries, η_Q), Extracted from the Spectra in Figure 7, and Suggested Assignments for Perovskite

	δ_1 (ppm), 9.4 T	δ_{iso} (ppm)	P_Q (MHz)	C_Q (MHz)	η_Q
O	75 (1)	108 (2)	5.1 (2)	5.1 (2)	0.1 (1)
Si		−193.0 (1)			

result for this phase,[16] where a signal was observed at −191.7 ppm in a 95% enriched material. The ^{17}O (54.2 MHz) MAS NMR spectrum of perovskite is shown in Figure 7b. It contains a line shape with features characteristic of second-order quadrupolar broadening and can be fitted fairly well by a single oxygen species with $C_Q = 5.1$ MHz and $\eta_Q = 0.1$, as shown in Table 6, and typical for a bridging oxygen. The STMAS spectrum of perovskite, shown in Figure 7c, and the isotropic projection shown in Figure 7d, also reveal a single resonance (at $\delta_1 \approx 75$ ppm), with no resolution of the two different oxygen species predicted by the crystal structure. The ^{17}O (81.4 MHz) MAS spectrum of perovskite is shown in Figure 7e. Here, in addition to the quadrupolar line shape, a broad, fairly featureless resonance is observed at lower δ. This signal is also present (between 20 and 50 ppm in δ_1) in the DQF-STMAS spectrum in Figure 7f, where its shape suggests a distribution of chemical shift parameters, indicating that it probably results from an amorphous phase. (Note that, unlike Figure 7c, there is no CT

→ CT autocorrelation diagonal present in this spectrum, as a double-quantum-filtered (DQF) pulse sequence has been used.) The broad peak is not as easily observed in the 9.4 T data, owing to the lower sensitivity, the presence of an autocorrelation diagonal, and the coincidental overlap with the perovskite signal at this field strength. While X-ray diffraction indicates that the sample is pure (except for Pt derived from the capsule), the method probes only the surface of the pellet, and the result is not necessarily representative of the bulk. This also applies to the akimotoite and majorite pellets that were analyzed by Raman spectroscopy. Furthermore, an amorphous phase may not be apparent with these techniques. It is worth noting that the ^{29}Si MAS spectrum of perovskite in ref 16 also contained an amorphous impurity. However, this would be below the detection level of the (non-enriched) ^{29}Si NMR spectrum in Figure 7.

Tables 1 and 2 give the calculated ^{29}Si and ^{17}O NMR parameters for perovskite. The ^{29}Si shift is in good agreement with the experimental results and is typical of an octahedrally coordinated silicon.[15] The ^{17}O results predict the two oxygen species to be extremely similar, with almost no difference in C_Q, a small difference in η_Q, and just a ppm difference in chemical shift. When combined in the correct intensity ratio (1:2 for O1 and O2, respectively), this would produce a line shape very similar to that observed experimentally, as shown in Figure 7b,e. However, any attempt to model the experimental MAS line shapes as the sum of two similar line shapes did not result in any significant or reproducible improvement in the fit. The calculated results support our assignment of the two distinct resonances in Figure 7e,f to two separate phases, rather than to the two different oxygen species expected in perovskite.

Discussion

The NMR parameters (both shielding and quadrupolar) provide insight into the local atomic environment, and much work has focused on establishing their relationship to a variety of structural parameters.[9−11,44,45] While many empirical correlations have been observed (usually within a series of similar compounds), the NMR parameters for a species depend in a complex manner upon a variety of structural features, including coordination number, the coordinating atoms and next-nearest neighbors, bond distances, bond angles, and symmetry. Figure 8a shows the dependence of the calculated ^{17}O chemical shift, δ_{iso}, on the average Si−O bond length for the polymorphs of $MgSiO_3$ (as given in Table 2) and Mg_2SiO_4.[22] There is a general positive correlation, as has been reported previously in the literature.[11,14] However, there is also an obvious dependence upon the oxygen environment, i.e., the directly coordinated atoms. For example, oxygen species coordinated to one Si and two Mg (SiMg2) have the shortest Si−O bond lengths but exhibit higher chemical shifts than some oxygen species coordinated to one Si and three Mg (SiMg3). Furthermore, for a comparatively small range of Si−O bond lengths, there is a large range of δ_{iso} for the "SiMg3" species. This illustrates the difficulty of spectral assignment and interpretation based on empirical correlations alone.

The assignment of the ^{17}O NMR spectra of the enstatite polymorphs suggested in the literature[14] differs from that found here using first-principles calculations. In the simplest case (protoenstatite), the bridging oxygen species (O3) can be easily identified, whereas differentiation of the two nonbridging oxygens, O1 and O2, is considerably more difficult. The previous experimental spectrum[14] exhibited two resonances with $\delta_{iso} \approx 39$ and 52 ppm, with very similar quadrupolar parameters. These were tentatively assigned on the basis that (i) generally ^{17}O δ_{iso} increases as the Si−O bond length increases and (ii) the O1 species in protoenstatite (coordinated to one Si and three Mg) is very similar to the O1 species in forsterite ($\delta_{iso} = 48$ ppm), while O2 (coordinated to one Si and two Mg) is very different. This led to an assignment of O2 and O1 in order of increasing chemical shift. The calculated parameters in Table

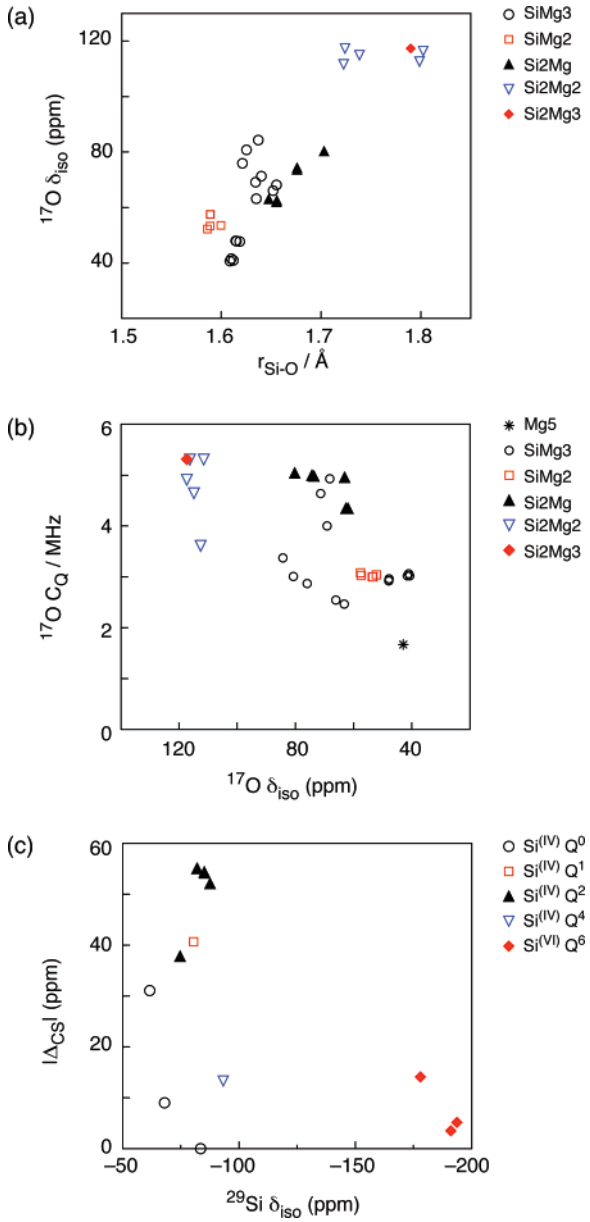

Figure 8. Dependence of (a) the calculated ^{17}O δ_{iso} on the average Si−O bond length, (b) the calculated ^{17}O C_Q on δ_{iso}, and (c) the modulus of the calculated ^{29}Si chemical shift anisotropy $|\Delta_{CS}|$ on the calculated ^{29}Si δ_{iso}, for polymorphs of $MgSiO_3$ and Mg_2SiO_4. Data for the latter are taken from ref 22. In (a) and (b), the key denotes the type and number of atoms coordinated to the oxygen; in (c), Si$^{(x)}$ denotes the coordination number, *x*, of the silicon and Q^n the number of bridging oxygen species, *n*, to which the Si$^{(IV)}$ are coordinated.

(44) Ashbrook, S. E.; Smith, M. E. *Chem. Soc. Rev.* **2006**, *35*, 718.
(45) Xue, X.; Stebbins, J. F. *Am. Mineral.* **1994**, *79*, 31.

2 suggest that this is not the case and that O1 actually has a lower δ_{iso} than O2, despite a longer Si−O bond length. Furthermore, although the immediate coordination environment of O1 in protoenstatite is similar to that of O1 in forsterite, a difference of ~8 ppm in chemical shift is predicted. For orthoenstatite and clinoenstatite, where the number of oxygen species is doubled, assignment becomes even more problematic. However, as shown in the previous section, the calculations enables a full assignment of both spectra.

There have been many attempts to relate the ^{17}O quadrupolar parameters (C_Q and η_Q) to local structure both through experimental investigation and cluster-type ab initio calculations.[44,45] Although a number of relationships have been determined, in particular many correlating C_Q/η_Q to the Si−O−Si bond angle,[44,45] in general these appear of limited applicability, relating specifically to a group of similar materials. Perhaps the most widely applicable observation is the increased C_Q usually associated with bridging compared to nonbridging oxygens.[11−13] This is attributed to the increased covalency (and hence lower ionicity) of the Si−O bonds for a bridging species as a result of a higher p orbital contribution. For $MgSiO_3$ and Mg_2SiO_4 silicates, there appears to be no particular correlation of either C_Q or η_Q with Si−O−Si angle or Si−O distance (not shown), although in general higher C_Q and lower η_Q values are found for larger Si−O−Si angles, in broad qualitative agreement with the literature.[44,45] However, the absence of any strong correlation probably reflects the range of complex structure types present, with differing numbers of coordinating atoms around many oxygens and the presence of both octahedral and tetrahedral silicate units. Figure 8b plots the calculated ^{17}O C_Q against δ_{iso} for the oxygen species in both sets of polymorphs. It was shown by Xue et al.[45] that, for a series of alkali silicates, such a plot was able to distinguish clearly environment types, particularly bridging and nonbridging oxygens. Broadly, this is also true for our magnesium silicates. Most nonbridging oxygens possess a low C_Q value, with the exceptions to this being the oxygen species in wadsleyite and ringwoodite.[19,22] Even in these unusual cases, the C_Q values for the nonbridging oxygens are lower than those of bridging oxygens in the same material. Figure 8b also shows that many nonbridging oxygens have a relatively low δ_{iso}. Those at higher δ_{iso} (above 75 ppm) are species in majorite, where oxygens are unusually connected to both six- and eight-coordinated magnesium species. This seems to produce a slightly increased ^{17}O δ_{iso}, as can also be observed in Figure 8a. Most C_Q values for the bridging oxygen species are between 4 and 6 MHz, again in broad agreement with the literature. In terms of chemical shift, they are separated into two distinct groups (with δ_{iso} = 55−80 and 105−120 ppm, respectively). Species with large chemical shifts occur in the polymorphs which contain octahedral silicate units (and correspondingly longer Si−O bond lengths). The C_Q of the single oxygen site in akimotoite (as noted in the previous section) is, however, somewhat smaller than expected. A detailed consideration of the immediate coordination environment reveals that this species has a much smaller Si−O−Si bond angle (99.2°) than the other bridging oxygens, in which the angles range from 120° to 150°. It should also be noted that, while only the modulus of C_Q has been compared to the experimental results, all C_Q values calculated here are, in fact, negative, with the exception of the oxygen species in akimotoite. This observation is in agreement with recent work by Grandinetti and coworkers,[46] where it was demonstrated that the magnitude and sign of the ^{17}O EFG in carbohydrates were dependent upon the C−O−H bond angle, with a change in sign observed when this angle was around 110°. It is hoped that further work might elucidate the factors controlling this variation in C_Q in much more detail.

For ^{29}Si NMR, a large number of empirical relationships between the isotropic chemical shift, δ_{iso}, and structural features, including coordination number, degree of polymerization (i.e., n in Q^n), electronegativity and bond strength of the next-nearest neighboring atoms, and Si−O−Si angles, have been observed experimentally.[9−11] The dependence of δ_{iso} on so many parameters restricts the applicability of many of these relationships to series of similar compounds and highlights the need for first-principles calculations to predict and assign spectra accurately. Figure 8c shows the modulus of the calculated chemical shift anisotropy ($|\Delta_{CS}|$) plotted against the calculated isotropic chemical shift δ_{iso} for the polymorphs of $MgSiO_3$ (Table 1) and Mg_2SiO_4.[22] The most obvious correlation is that of the isotropic shift with the Si coordination number, with six-coordinate silicon species ($Si^{(VI)}$) exhibiting considerably more negative values of δ_{iso} than the four-coordinate species ($Si^{(IV)}$). The various four-coordinated Q^n species fall within the ranges predicted in the literature[9−11] (−60 to −90 ppm for Q^0, −72 to −85 ppm for Q^1, −80 to −105 ppm for Q^2, and −100 to −115 ppm for Q^4 species). However, this general increase in chemical shift as n decreases is not immediately apparent from Figure 8c, since the parameter values are also affected by structural differences between the species. For example, the Q^0 species in ringwoodite appear at a lower δ_{iso} than the Q^1 species in wadsleyite, although both fall within their respective literature ranges.[19,22] Similarly, the Q^2 species in majorite has a higher δ_{iso} than both the Q^0 and Q^1 silicons in ringwoodite and wadsleyite, although again all fall within the observed experimental ranges. It is also noticeable that the Q^4 species in majorite exhibits a higher shift (−94 ppm) than expected. However, for the three four-coordinate silicon species in majorite, there is a gradual increase in chemical shift as n increases from 0 to 2 and to 4. The unequal spacing of these three resonances has been mentioned previously in the literature and suggested to result from the presence of silicons connected (through oxygen species) to high- (six-)-coordinate silicon and six- and eight-coordinate Mg.[15] This agrees with a previous observation that the ^{29}Si δ_{iso} increases as the electrostatic bond strength decreases (a direct result of increasing the coordination number of the nearby atoms).[9,10] For the six-coordinate silicons, similar shifts are observed for both perovskite and majorite, but that in akimotoite is slightly larger. This perhaps results from the markedly different Si−O−Si bond angle (99.2°).

The calculated ^{29}Si $|\Delta_{CS}|$ values range between 0 and 55 ppm, with the smallest values exhibited by the (arguably more symmetrical) $Q^0$and Q^4 species, while the largest values are found for Q^2 silicons. The only experimental values of Δ_{CS} and η_{CS} in the literature are for enstatite, and these are in good agreement with our calculated results.[9] It is suggested in ref 16 that the ^{29}Si Δ_{CS} in perovskite was very small (as it could not be determined from a Herzfeld−Berger-type analysis, even at

(46) Sefzik, T. H.; Houseknecht, J. B.; Clark, T. M.; Prasad, S.; Lowary, T. L.; Gan, Z.; Grandinetti, P. J. *Chem. Phys. Lett.* **2007**, *434*, 312.

slow MAS rates). This is confirmed in our calculations, where a Δ_{CS} of only ~3.6 ppm is predicted.

This work and our previous study on the polymorphs of Mg_2SiO_4[18,19,22] illustrate how the calculated NMR parameters for each O and Si site in a crystal structure closely correspond to parameters determined experimentally, allowing confident assignment of NMR resonances to crystallographic species. This provides the foundation for investigating the incorporation of H, as hydroxyl groups, at disordered defect sites in these phases. The aim is to determine the O to which the H is coordinated from changes in NMR parameters of a particular species, from the appearance of new resonances, or through the development of techniques such as $^{17}O-^{1}H$ cross-polarization. Furthermore, noting the sensitivity of NMR parameters to a whole range of structural variables, it is hoped that the length and orientation of the OH bond may be constrained by the computational model of the defect. This will, in turn, help define the hydrogen-bonding network and "strength" of the hydrated mineral, with implications for a range of geophysical properties such as deformation and rheology (response to dislocation creep) and seismic wave speeds (the effect on the elastic moduli). An investigation of the hydrated polymorphs of $MgSiO_3$ and Mg_2SiO_4 is the subject of ongoing research.

Conclusions

The ^{17}O and ^{29}Si NMR parameters for six polymorphs of $MgSiO_3$ were obtained by a combination of variable-field high-resolution NMR and first-principles calculations. For the lower pressure polymorphs (ortho-, clino-, and protoenstatite), the use of first-principles calculations enabled the resolved peaks in high-resolution MQMAS ^{17}O NMR spectra to be assigned to the crystallographic oxygen species. These assignments differ from those suggested in previous work, which was based almost solely upon empirical correlations. We have presented the first ^{17}O NMR spectra of the high-pressure $MgSiO_3$ polymorphs (akimotoite, majorite, and perovskite) and confirmed previous ^{29}Si results in the literature. Both ^{17}O STMAS and MQMAS NMR spectroscopy were used at two different field strengths to resolve the distinct oxygen species and obtain accurate quadrupolar and shielding parameters. The use of first-principles calculations also enabled full assignments of all these spectra. In addition, this work has provided an opportunity to reconsider the dependence of the NMR parameters on local structure. In particular, we have found that, although there is a general correlation of increasing ^{17}O chemical shift with increasing Si−O bond length, the shift observed also depends crucially on the other aspects of the coordination environment. These effects cannot be distinguished empirically with the available data but can be reproduced computationally.

Acknowledgment. We are grateful to the Leverhulme Trust for financial support (grant no. F00179AH) and to the Royal Society for a Dorothy Hodgkin Research Fellowship (to S.E.A.). High-pressure syntheses were performed under the EU "Research Infrastructure: Transnational Access" (RITA) Programme (Contract No. 505320—The Structure and Properties of Materials at High Pressure). We thank Dr. Stefan Steuernagel and Bruker Biospin GmbH for assistance with and access to the 600 Avance III NMR spectrometer. This work has also made use of resources provided by the EaStCHEM Research Computing Facility (http://www.eastchem.ac.uk/rcf). This facility is partially supported by the eDIKT initiative (http://www.edikt.org).

JA074428A